PLOS ONE

RESEARCH ARTICLE

TGF-β inhibition can overcome cancer primary resistance to PD-1 blockade: A mathematical model

Nourridine Siewe[1]*, **Avner Friedman**[2]

1 School of Mathematical Sciences, College of Science, Rochester Institute of Technology, Rochester, New York, United States of America, **2** Department of Mathematics, Mathematical Biosciences Institute, The Ohio State University, Columbus, Ohio, United States of America

* nxssma@rit.edu

Citation: Siewe N, Friedman A (2021) TGF-β inhibition can overcome cancer primary resistance to PD-1 blockade: A mathematical model. PLoS ONE 16(6): e0252620. https://doi.org/10.1371/journal.pone.0252620

Editor: Joseph Najbauer, University of Pécs Medical School, HUNGARY

Received: January 30, 2021

Accepted: May 18, 2021

Published: June 1, 2021

Data Availability Statement: All relevant data are within the manuscript and its Supporting information files.

Funding: This research was supported by the Dean's Research Initiative Grant #15874 of the College of Science at Rochester Institute of Technology. This work was also supported by the Mathematical Biosciences Institute of The Ohio State University. There was no additional external funding received for this study.

Competing interests: The authors have declared that no competing interests exist.

Abstract

Immune checkpoint inhibitors have demonstrated, over the recent years, impressive clinical response in cancer patients, but some patients do not respond at all to checkpoint blockade, exhibiting primary resistance. Primary resistance to PD-1 blockade is reported to occur under conditions of immunosuppressive tumor environment, a condition caused by myeloid derived suppressor cells (MDSCs), and by T cells exclusion, due to increased level of T regulatory cells (Tregs). Since TGF-β activates Tregs, TGF-β inhibitor may overcome primary resistance to anti-PD-1. Indeed, recent mice experiments show that combining anti-PD-1 with anti-TGF-β yields significant therapeutic improvements compared to anti-TGF-β alone. The present paper introduces two cancer-specific parameters and, correspondingly, develops a mathematical model which explains how primary resistance to PD-1 blockade occurs, in terms of the two cancer-specific parameters, and how, in combination with anti-TGF-β, anti-PD-1 provides significant benefits. The model is represented by a system of partial differential equations and the simulations are in agreement with the recent mice experiments. In some cancer patients, treatment with anti-PD-1 results in rapid progression of the disease, known as hyperprogression disease (HPD). The mathematical model can also explain how this situation arises, and it predicts that HPD may be reversed by combining anti-TGF-β to anti-PD-1. The model is used to demonstrate how the two cancer-specific parameters may serve as biomarkers in predicting the efficacy of combination therapy with PD-1 and TGF-β inhibitors.

1 Introduction

Immune checkpoint inhibitors, introduced in recent years, have demonstrated impressive clinical response in cancer patients, although resistance may develop over time. But some patients do not respond at all to checkpoint blockade, exhibiting, what is called, primary resistance. Mechanisms of adaptive resistance to PD-1 blockade and potential therapies to overcome it are reviewed in [1–5], and of primary resistance in [3–5]. In particular, primary

resistance is reported to occur under conditions of immunosuppressive tumor environment, including effective T cells exclusion [4, 5]. Such environment is often caused by increased level of T regulatory cells (Tregs). Indeed, as reported in [6, 7], PD-1 expression balance between effective T cells and Tregs predicts the efficacy of PD-1 blockade therapy. In clinical study of patients with melanoma, PD-1 blockade resulting in decline of $PD1^+$ Tregs predicted more favorable outcome [8]

In some cancer patients, treatment with anti-PD-1 resulted in rapid progression of tumor, known as hyperprogression disease (HPD) [8–10]. Recent reviews of HPD in cancer patients appeared in [11–13], and, of biomarkers for HPD, in [14]. Although the mechanism of HPD is unknown, it has been noted that HPD is associated with increased levels of MDSC and Treg cells [11, 14]. Motivated by the observation that HPD occurs in approximately 10% of anti-PD-1 monoclonal anti-body (mAb)-treated advanced gastric cancer patients, Kamada et al. [15] conducted mice experiments with gastric cancer. They demonstrated that PD-1 blockade activated and expanded tumor infiltration of $PD\text{-}1^+$ Tregs to overwhelm tumor $PD\text{-}1^+$ effective T cells, as cancer underwent rapid progression.

TGF-β is a pleiotropic cytokine that could suppress immune response by regulating Tregs [16]. Hence TGF-β blockade is likely to enhance immune-checkpoint therapy [17]. Mariathasan et al. [18] and Tauriello et al. [19] identified TGF-β signaling in tumor microenvironment as a determinant of tumor T cell role in affecting poor response to PD-1/PD-L1 blockade. They demonstrated, in mouse models, that combining TGF-β inhibition with immune checkpoint blockade induces complete and durable response to otherwise unresponsive tumor; see also reveiw article [20]. Sow et al. [21] found that combined inhibition of TGF-β signaling and PD-L1 is differentially effective in mouse model.

Streel et al. [22] and Martin et al. [23] have recently demonstrated, in several mouse models, that TGF-β inhibition overcomes primary resistance to PD-1 blockade. More precisely, in some cancers, PD-1 inhibition does not decrease tumor volume, but, in combination with anti-TGF-β, PD-1 blockade significantly improves outcome of treatment compared to treatment with anti-TGF-β alone. In this paper, we develop a mathematical model that explains these experimental results in [15, 22, 23] in terms of two cancer-specific parameters that may serve as cancer biomarkers.

The model is based on two important observations:

(i) TGF-β (T_β) inhibits the killing rate of cancer cells by $CD8^+$ T cells [24]; we represent this inhibition by a factor $1/(1+\zeta_{T_\beta}T_\beta)$, for some constant ζ_{T_β}.

(ii) The complex Q = PD-1/PD-L1 induces change from pro-inflammatory $CD4^+$ T cells (T_1) to regulatory T cells (T_r) [25, 26], at rate modeled by $\lambda_{T_1T_r}T_1Q/(K_Q+Q)$, where K_Q and $\lambda_{T_1T_r}$ are constants.

Anti-PD-1 increases the activation of $CD8^+$ T cells (T_8). On the other hand, T_β contributes to the proliferation of T_r [27–28], possibly resulting in only minimal increase (T_8).

PD-1 blockade increases the proliferation rate of T_1. If T_1 were fixed, the loss rate $\lambda_{T_1T_r}T_1Q/(K_Q+Q)$ of T_1 (to T_r) will also decrease. But since the proliferation of T_1 has increased by the PD-1 blockade, the product $T_1\,Q/(K_Q{+}Q)$ may conceivably increase; in this case the rate of change $\lambda_{T_1T_r}T_1Q/(K_Q+Q)$ from T_1 to T_r will increase, and, if $\lambda_{T_1T_r}$ is sufficiently large, the T_r inhibition of T_8 may result in loss of T_8, and thus in hyperprogression of cancer.

Myeloid cells play an important immunosuppressive role in the tumor microenvironment. They include MDSCs, M2 macrophages and M2-like TAMs (tumor associated macrophages)

[29]. MDSCs secrete IL-10 [30, 31] and TGF-β [28, 32, 33]; M2 macrophages secrete IL-10 [34, 35], and TAMs and M2 macrophages secrete TGF-β [36]. For simplicity we shall represent these three types of myeloid populations by one variable, designated by M_2, and will refer to it as MDSC or M2.

The mathematical model is represented by a system of partial differential equations within the tumor compartment. The species in the model include immune cells, $CD8^+$ and $CD4^+$-Th1 T cells, Tregs, immunosuppressive M2 macrophages and pro-inflammatory macrophages M1, and dendritic cells. They also include cytokines that play important role in the interactions among immune cells and cancer cells: CCL2 (MCP-1) and interleukins IL-2, IL-10 and IL-12. CCL2 is produced by cancer cells [37], and it attracts MDSCs into the tumor compartment [38–40]. IL-2 is produced by Th1 cells [41] and it enhances the proliferation of T_1 and T_8, but also T_r, so its effect in clinical trials is not always predictable [42]. IL-12 is produced by dendritic cells and it activates T_1 and T_8 cells [43]. IL-10 is produced by MDSCs, M2 macrophages and cancer cells [30, 31]. Both IL-10 and T_r inhibit the activation of T_1 and T_8 by IL-12 [31]. The cancer-specific parameters $\lambda_{T_1T_r}$ and ζ_{T_β} play a critical role in the model simulations, and are adjusted in order to establish agreement with the experimental results of Streel et al. [22], Martin et al. [23], and Kamada et al. [15]. The model is then used to demonstrate how various other choices of these two parameters determine the efficacy of combination therapy with anti-PD-1 and anti-TGF-β, and how these parameters may serve as prediction biomarkers.

2 Mathematical model

The mathematical model is based on the network shown in Fig 1. Table 1 lists the variables of the model in units of g/cm^3. We assume that all species X_i, ($i = 1, \ldots, n$) are dispersing (or diffusing) with a coefficient δ_{X_i}, and are dying (or degrading) at rate μ_{X_i}; cells also undergo advection velocity **u** that is associated with internal pressure in the tumor compartment, see S1 File.

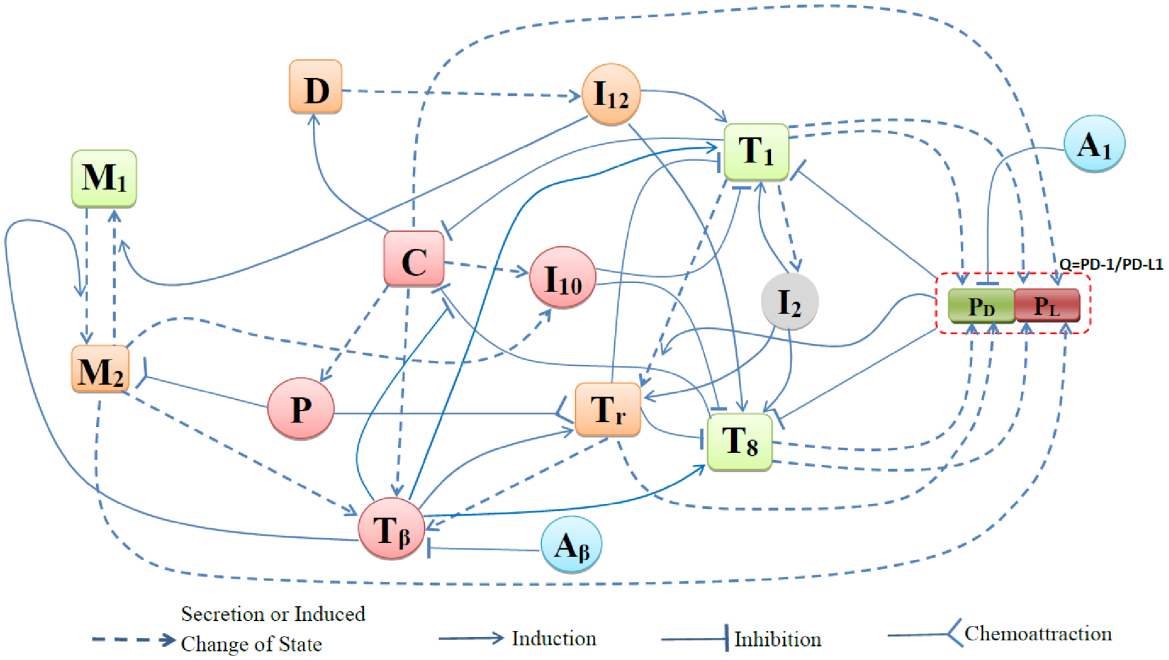

Fig 1. Network describing the interactions between cells and cytokines under treatment with anti-PD-1 and anti-TGF-β.

https://doi.org/10.1371/journal.pone.0252620.g001

Table 1. Variables of the model. All concentrations are in units of g/cm^3.

Variables	Descriptions	Variables	Descriptions
M_1	density of M1 macrophages	M_2	density of MDSCs
D	density of dedritic cells	T_1	density of CD4$^+$ T/Th1 cells
T_8	density of CD8$^+$ T cells	T_r	density of Treg cells
C	density of cancer cells		
I_2	concentration of IL-2	I_{10}	concentration of IL-10
I_{12}	concentration of IL-12	P	concentration of CCL2 (MCP-1)
T_β	concentration of TGF-β	P_D	concentration of PD-1
P_L	concentration of PD-L1	Q	concentration of PD-1/PD-L1
A_1	concentration of anti-PD-1	A_β	concentration of anti-TGF-β

https://doi.org/10.1371/journal.pone.0252620.t001

We write the equation for cells X_i in the form

$$\frac{\partial X_i}{\partial t} + \nabla \cdot (\mathbf{u}X_i) - \delta_{X_i}\nabla^2 X_i = F_{X_i}(X_1, \ldots, X_n)$$

where ∇^2 is the Laplace operator $\nabla\cdot$grad, or $\sum_{j=1}^{3}\frac{\partial^2}{\partial x_j^2}$. In modeling the structure of F_{X_i} we use, for simplicity, the linear mas conservation law, that is, if X_j+$X_k \rightarrow X_m$ then the rate by which X_m is formed, or X_j is lost, is $mX_j X_k$ where m is a positive parameter. In a process where X_i is activated by cytokine X_j, X_j represents molecules that are bound and internalized by X_i, and this internalization may be limited owing to the limited rate of receptor recycling. We then represent the rate of activation by the Michaelis-Menten law $mX_i(X_j/(K+X_j))$ for some positive parameters m, K. A term of the form $mX_i/(1+X_j/K)$ means that X_j inhibits the growth of X_i. Finally, an expression of the form $\nabla\cdot(X_i\chi\nabla X_j)$ means that X_i is moving by chemotaxis in the direction of the gradient of chemoattractant X_j with chemotactic force χ, where χ is a positive parameter.

2.1 Equation for tumor cells (C)

We assume a logistic growth for cancer cells with carrying capacity C_M, to account for space competition among these cells. Cancer cells are killed by CD8$^+$ T cells, a processed inhibited by the pleiotropic cytokine TGF-β [24], represented by the factor $\frac{1}{1+\zeta_{T_\beta}T_\beta}$. We write the equation for C in the following form:

$$\frac{\partial C}{\partial t} + \nabla \cdot (\mathbf{u}C) - \delta_C\nabla^2 C = \underbrace{\lambda_C C\left(1 - \frac{C}{C_M}\right)}_{\text{Growth of cancer cells}} - \underbrace{\frac{\mu_{T_8C}}{1+\zeta_{T_\beta}T_\beta}T_8 C}_{\text{killing by } T_8} - \underbrace{\mu_C C}_{\text{death}}. \quad (1)$$

2.2 Equation for M1 macrophages (M_1)

The equation for M1 macrophages has the following form:

$$\frac{\partial M_1}{\partial t} + \nabla \cdot (\mathbf{u} M_1) - \delta_M \nabla^2 M_1 = \underbrace{\lambda_{M_1} M_0 \frac{P}{K_P + P}}_{\text{activation by CCL2}} - \underbrace{\nabla \cdot (\chi_P M_1 \nabla P)}_{\text{chemoattraction by CCL2}} + \underbrace{\lambda_{M_2 M_1} M_2 \frac{I_{12}}{K_{I_{12}} + I_{12}}}_{M_2 \to M_1 \text{ by IL-12}} - \underbrace{\lambda_{M_1 M_2} M_1 \frac{T_\beta}{K_{T_\beta} + T_\beta}}_{M_1 \to M_2 \text{ by TGF-}\beta} - \underbrace{\mu_{M_1} M_1}_{\text{death}} \tag{2}$$

where the first term on the right-hand side represents a source of macrophages differentiated from monocytes that are activated by CCL2 (P) and the second term represents chemoattraction of M_1 by CCL2 [44]. The third and fourth terms on the right-hand side represent phenotype changes from M_2 to M_1 induced by IL-12, and from M_1 to M_2 induced by TGF-β [44, 45].

2.3 Equation for MDSCs (M_2)

Tumor recruits macrophages and "educates" them to become tumor-associated-macrophages (TAMs), which behave like MDSCs [46, 47]; MDSCs are chemotactically attracted by CCL2 [38–40]. The equation for M_2 is given by:

$$\frac{\partial M_2}{\partial t} + \nabla \cdot (\mathbf{u} M_2) - \delta_M \nabla^2 M_2 = \underbrace{\lambda_{M_2} M_0 \frac{P}{K_P + P}}_{\text{activation by CCL2}} - \underbrace{\nabla \cdot (\chi_P M_2 \nabla P)}_{\text{chemoattratced by CCL2}} - \underbrace{\lambda_{M_2 M_1} M_2 \frac{I_{12}}{K_{I_{12}} + I_{12}}}_{M_2 \to M_1 \text{ by IL-12}} + \underbrace{\lambda_{M_1 M_2} M_1 \frac{T_\beta}{K_{T_\beta} + T_\beta}}_{M_1 \to M_2 \text{ by TGF-}\beta} - \underbrace{\mu_{M_2} M_2}_{\text{death}}. \tag{3}$$

2.4 Equation for CD4$^+$ T/Th1 cells (T_1)

The pleiotropic cytokine TGF-β contributes to the development of naive CD4$^+$ T cells, T_{10} [48]. Naive CD4$^+$ T cells differentiate into Th1 cells under IL-12 inducement [41, 49], and this process is inhibited by IL-10 and Tregs. The proliferation of activated CD4$^+$ T cells is enhanced by IL-2 [42]. Activation and proliferation of T_1 cells are inhibited by the complex PD-1/PD-L1 (Q), represented by the factor $\frac{1}{1+Q/\hat{K}_{TQ}}$. The complex Q also mediates phenotype change from Th1 cells to Treg cells [25, 26], by a factor $\lambda_{T_1 T_r} \frac{Q}{K_Q + Q}$; we consider the parameter $\lambda_{T_1 T_r}$ to be cancer-specific. Hence T_1 satisfies the following equation:

$$\begin{aligned} &\frac{\partial T_1}{\partial t} + \underbrace{\nabla \cdot (\mathbf{u} T_1)}_{\text{advection}} - \underbrace{\delta_T \nabla^2 T_1}_{\text{diffusion}} = \\ &\left(\lambda_{T_1 I_{12}} T_{10} \underbrace{\left(1 + \frac{T_\beta}{K_{T_\beta} + T_\beta}\right)}_{T_\beta\text{-augmented activation}} \underbrace{\frac{I_{12}}{K_{I_{12}} + I_{12}}}_{\text{activation by IL-12}} \cdot \underbrace{\frac{1}{1 + I_{10}/\hat{K}_{TI_{10}}}}_{\text{inhibition by IL-10}} \cdot \underbrace{\frac{1}{1 + T_r/\hat{K}_{TT_r}}}_{\text{inhibition by Tregs}} + \right. \\ &\left. \underbrace{\lambda_{T_1 I_2} T_1 \frac{I_2}{K_{I_2} + I_2}}_{\text{IL-2-induced proliferation}} \right) \times \underbrace{\frac{1}{1 + Q/\hat{K}_{TQ}}}_{\text{inhibition by } Q} - \underbrace{\lambda_{T_1 T_r} T_1 \frac{Q}{K_Q + Q}}_{Q\text{-induced } T_1 \to T_r \text{ transition}} - \underbrace{\mu_{T_1} T_1}_{\text{death}}. \end{aligned} \tag{4}$$

2.5 Equation for activated CD8$^+$ T cells (T_8)

The cytokine TGF-β contributes to the development of inactive CD8$^+$ T cells, T_{80} [48]. Inactive CD8$^+$ T cells are activated by IL-12 [41, 49], and this process is resisted by IL-10 and Treg cells [27, 31]. IL-2 enhances the proliferation of activated CD8$^+$ T cells [42]. Both processes of activation and proliferation are inhibited by PD-1/PD-L1, by the factor $\frac{1}{1+Q/\hat{K}_{TQ}}$. Hence, T_8 satisfies the following equation:

$$\frac{\partial T_8}{\partial t} + \nabla \cdot (\mathbf{u} T_8) - \delta_T \nabla^2 T_8 = \left(\lambda_{T_8 I_{12}} T_{80} \underbrace{\left(1 + \frac{T_\beta}{K_{T_\beta} + T_\beta}\right)}_{T_\beta\text{-augmented activation}} \underbrace{\frac{I_{12}}{K_{I_{12}} + I_{12}}}_{\text{activation by IL-12}} \cdot \underbrace{\frac{1}{1 + I_{10}/\hat{K}_{TI_{10}}}}_{\text{inhibition by IL-10}} \cdot \underbrace{\frac{1}{1 + T_r/\hat{K}_{TT_r}}}_{\text{inhibition by Tregs}} + \underbrace{\lambda_{T_8 I_2} T_8 \frac{I_2}{K_{I_2} + I_2}}_{\text{IL-2-induced proliferation}} \right) \times \underbrace{\frac{1}{1 + Q/\hat{K}_{TQ}}}_{\text{inhibition by } Q} - \underbrace{\mu_{T_8} T_8}_{\text{death}}. \tag{5}$$

2.6 Equation for Tregs (T_r)

Naive CD4$^+$ T cells differentiate into Tregs under activation by Fox3+ transcription factor, a process enhanced by TGF-β [27, 28]. The activated Tregs are recruited into tumor by tumor-derived immunosuppressive cytokines IL-6 and CCL2 (P) [38–40]; for simplicity, we represent both cytokines by CCL2. IL-2 enhances the proliferation of Tregs within the tumor [42] Representing this chemoattraction by $\nabla\cdot(\chi_P T_r \nabla P)$, we get the following equation for T_r:

$$\frac{\partial T_r}{\partial t} + \nabla \cdot (\mathbf{u} T_r) - \delta_T \nabla^2 T_r = \underbrace{\lambda_{T_r T_\beta} T_{10} \frac{T_\beta}{K_{T_\beta} + T_\beta}}_{T_\beta\text{-enhanced naive T cells activation}} + \underbrace{\lambda_{T_1 T_r} T_1 \frac{Q}{K_Q + Q}}_{Q\text{-induced } T_1 \to T_r \text{ transition}} + \underbrace{\lambda_{T_r I_2 T_r} \frac{I_2}{K_{I_2} + I_2}}_{\text{IL-2-induced proliferation}} - \underbrace{\nabla \cdot (\chi_P T_r \nabla P)}_{\text{chemoattraction by CCL2/MCP-1}} - \underbrace{\mu_{T_r} T_r}_{\text{death}}, \tag{6}$$

where the second term in the right-hand side is the same as in Eq (4).

2.7 Equation for TGF-β (T_β)

When anti-TGF-β drug is applied, TGF-β is depleted at a rate proportional to A_β, and the equation for T_β takes the following form:

$$\frac{\partial T_\beta}{\partial t} - \delta_{T_\beta} \nabla^2 T_\beta = \underbrace{\lambda_{T_\beta C} C + \lambda_{T_\beta M_2} M_2 + \lambda_{T_\beta T_r} T_r}_{\text{secretion by } C,\ M_2 \text{ and } T_r} - \underbrace{\mu_{T_\beta} T_\beta}_{\text{degradation}} - \underbrace{\mu_{A_\beta T_\beta} T_\beta A_\beta}_{\text{depletion by anti-TGF-}\beta}. \tag{7}$$

The equations for I_2, I_{10}, I_{12}, P, as well as the equations for P_D and P_L are given in S1 File, and we take

$$Q = \sigma P_D P_L, \tag{8}$$

for some parameter σ.

2.8 Equation for anti-PD-1 (A_1)

In mice experiments in [23], anti-PD-1 was injected, intraperitoneally twice a week, begining t_0 days after tumor cells implantation, and ending at day t_1; in [22] the drug was administered daily. We approximate the effective source of the drug by taking it to be a constant, γ_{A_1}, so that

$$c_{A_1}(t) = \begin{cases} \gamma_{A_1}, & \text{if } t_0 \le t \le t_1 \\ 0, & \text{otherwise.} \end{cases} \tag{8}$$

The drug is depleted in the process of blocking PD-1, so that

$$\frac{\partial A_1}{\partial t} - \delta_{A_1}\nabla^2 A_1 = \underbrace{c_{A_1}(t)}_{\text{source}} - \underbrace{\mu_{P_D A_1} P_D A_1}_{\text{depletion through blocking PD}-1} - \underbrace{\mu_{A_1} A_1}_{\text{degradation}} \tag{9}$$

2.9 Equation for anti-TGF-β (T_β)

In [22, 23], anti-TGF-β was administered weekly for the same periods $t_0 \le t \le t_1$ as in (8). We again approximate the effective level of the drug by taking

$$c_{A_\beta}(t) = \begin{cases} \gamma_{A_\beta}, & \text{if } t_0 \le t \le t_1 \\ 0, & \text{otherwise} \end{cases} \tag{10}$$

where γ_{A_β} is some constant. The drug A_β is depleted in the process of blocking TGF-β, so that

$$\frac{\partial A_\beta}{\partial t} - \delta_{A_\beta}\nabla^2 A_\beta = \underbrace{c_{A_\beta}(t)}_{\text{source}} - \underbrace{\mu_{T_\beta A_\beta} T_\beta A_\beta}_{\text{depletion through blocking TGF}-\beta} - \underbrace{\mu_{A_\beta} A_\beta}_{\text{degradation}} \tag{11}$$

2.10 Equation for cells velocity (u). The velocity **u** is determined by the condition that the combined density of all cells in the tumor compartment is constant; see S1 File.

To simplify the computations, we assume that the tumor is spherical and that all the densities and concentrations are radially symmetric, that is, functions of (r, t), $0 \le r \le R(t)$ where $r = R(t)$ is the boundary of the tumor, and that $\mathbf{u} = u(r, t)\mathbf{e}_r$, where $\mathbf{e}_r$ is the unit radial vector.

2.11 Equation for free boundary (R). We assume that the free boundary $r = R(t)$ moves with the velocity of cells, so that

$$\frac{dR(t)}{dt} = u(R(t), t). \tag{12}$$

We complement the system by prescribing initial and boundary conditions; see S1 File.

3 Results

All the computations were done using Python 3.5.4. The parameter values of the model equations are estimated in and are listed in S1 File. The technique used in the simulations is also described in S1 File.

3.1 Mouse models and simulations

We define the efficacy of treatment by

$$\text{efficacy} = \frac{\text{tumor volume with no treatment} - \text{tumor volume under treatment}}{\text{tumor volume with no treatment}} \times 100\%, \quad (13)$$

where both volumes are measured at the last day of treatment. We refer to efficacy as the relative difference (in tumor volume) of treatment to no treatment, in percentage. Negative efficacy means that treatment resulted in increase (rather than decrease) in tumor volume.

Streel et al. [22] and Martin et al. [23] performed mice experiments with different types of cancer, treated with combinations of anti-PD-1 and anti-TGF-β. In Streel et al. [22] (Fig. 2b), mice were implanted with colon cancer cells and treatment began 6 days after infection. The tumor volume in each mouse was measured regularly for 45 days and reported accordingly. They found that there was almost no reduction in the tumor size when treatment was with anti-PD-1 alone, but the tumor volume reduced significantly when anti-PD-1 was combined with anti-TGF-β. Our simulations in Fig 2A show the volume of the tumor in the cases of no treatment and treatment with various combinations of anti-PD-1 and anti-TGF-β. We see that while anti-PD-1 as a single agent does not reduce the cancer volume growth, when given in combination with anti-TGF-β, the growth of the tumor volume is significantly decreased; this is in agreement with Fig. 2b in [22]

In the experiments conducted by Martin et al. [23], mice were implanted with cells from bladder cancer, melanoma or breast cancer, and then treated with anti-PD-1 as a single agent, or with combination of anti-PD-1 and anti-TGF-β. Starting treatment at day 14 post-infection, Martin et al. found, as in [22], that in the case of breast cancer ([23] Fig 4B, 4C) and bladder cancer ([23] Fig 4G, 4H), with anti-PD-1 alone there was hardly any reduction in the tumor volume, but in combination with anti-TGF-β, anti-PD-1 reduced tumor volume significantly; Fig 2C and 2D are in agreement with these results. On the other hand, in the case of melanoma ([23] Fig 4D, 4E), there was primary resistance to anti-PD-1; Fig 2B is in agreement with this result. Note that the cancer-specific parameter ζ_{T_β} in Fig 2B is much smaller than the corresponding parameter in Fig 2A, 2D and 2E.

Note that the parameters $\lambda_{T_1T_r}$ and ζ_{T_β} are the same in Fig 2A, 2C and 2D, but the profiles are taken for different time durations (45, 56 and 32 days, respectively), and this accounts for the somewhat different impressions one may get of the tumor volume growth.

In mice experiments with gastric cancer, Kamada et al. [15] administered anti-PD-1 as a single agent and compared the tumor volume in this case to the tumor volume in the control (no-drug) case. They observed that the tumor volume with anti-PD-1 exceeded the tumor volume in the control case (Fig 6B, 6C in [15]). The simulations in Fig 2E show the same qualitative results. Notice that in these simulations, the parameter ζ_{T_β} is the same as in Fig 2A, 2C and 2D, but $\lambda_{T_1T_r}$ is much larger than in these figures.

Fig 2E shows also the effect of anti-PD-1 on tumor treated with anti-TGF-β: In the first few weeks, tumor volume slightly increases (hyperprogression of cancer) but later on it decreases, and by day 45 it is significantly decreased under the combined therapy.

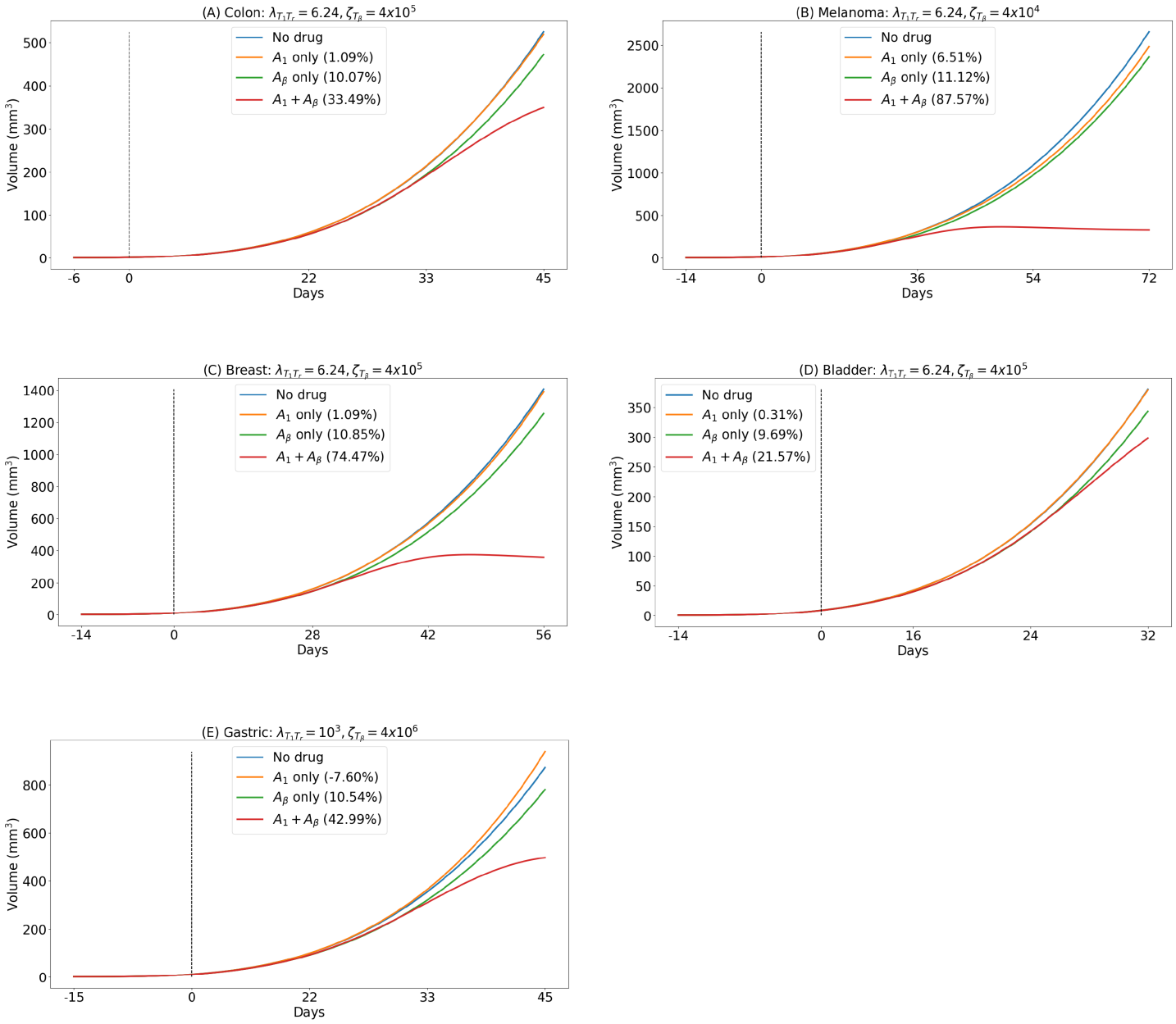

Fig 2. Tumor volume under various combinations with anti-PD-1 and anti-TGF-β. The "%" represents the difference, in volume, of treatment to no treatment, in percentage. All parameters are as in S1 File, with $\gamma_{A_1} = 10^{-8}$ g/cm$^3 \cdot$ d and $\gamma_{A_\beta} = 2 \times 10^{-6}$ g/cm$^3 \cdot$ d. (A) Colon cancer: treatment starts at day 6 which corresponds to the schedule in [22]. (B) Melanoma cancer: treatment starts at day 14 as in [22]. (C) Breast cancer: treatment starts at day 14 as in [23]. (D) Bladder cancer: treatment starts at day 14 which corresponds to the schedule in [23]. (E) Gastric cancer: treatment starts at day 15 which corresponds to the schedule in [15].

https://doi.org/10.1371/journal.pone.0252620.g002

3.2 Tumor volume hyperprogression

The simulations in Fig 2 suggest that hyperprogression of cancer under PD-1 inhibition depends on the parameters $\lambda_{T_1T_r}$ and ζ_{T_β}. Fig 3 shows tumor volume at day 45 for pairs of parameters $(\zeta_{T_\beta}, \lambda_{T_1T_r})$ in the range $0 < \zeta_{T_\beta} < 1.5 \times 10^6$ cm^3/g, $0 < \lambda_{T_1T_r} < 5 \times 10^4$ d^{-1}. The color column scales the efficacy, that is, the percentage of increase/decrease of tumor volume

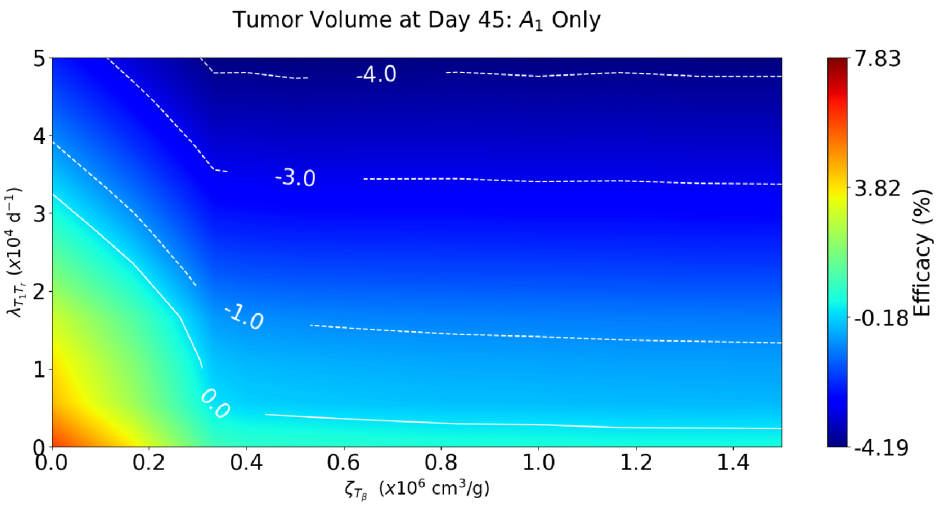

Fig 3. Combined effect of cancer-specific parameters $\lambda_{T_1T_r}$ and ζ_{T_β}, under treatment with anti-PD-1, at $\gamma_{A_1} = 10^{-8}$ g/cm^3 · d. The color column indicates relative difference of the tumor volume at day 45. Negative values represent parameter ranges of tumor hyperprogression.

https://doi.org/10.1371/journal.pone.0252620.g003

relative to the control case; the drug level is taken to be $\gamma_{A_1} = 10^{-8}$ g/cm^3 · d. We see that (i) negative efficacy (hyperprogression) increases with both $\lambda_{T_1T_r}$ and ζ_{T_β}, and (ii) efficacy is positive when either $\lambda_{T_1T_r}$ or ζ_{T_β} is small. A monotone decreasing curve of the form $\lambda_{T_1T_r} = f(\zeta_{T_\beta})$ separates the regions of positive and negative efficacies.

Kamada et al. [15] (Fig. 5F) also measured the level of Tregs under treatment with anti-PD-1 as single agent, and compared it with the corresponding level of Tregs in the control case. They found that Tregs level increased by 1/3 more than their corresponding level in the control case. The simulations in Fig 4 show the same level of increase of Tregs under treatment with anti-PD-1, with cancer-specific parameters $\zeta_{T_\beta} = 4 \times 10^6$ cm^3/g and $\lambda_{T_1T_r} = 10^3$ d^{-1}. Fig 4 also shows that the Tregs level is very low under treatment with anti-TGF-β, but it increases significantly (although it remains below the control case) in combination with anti-PD-1.

3.3 Efficacy maps

In order to see how the cancer-specific parameters affect the efficacy of treatment, we took 9 pairs $(\lambda_{T_1T_r}, \zeta_{T_\beta})$ as in Fig 5 and for each pair, we simulated the model under combination therapy with $(\gamma_{A_\beta}, \gamma_{A_1})$ that vary in the region $0 < \gamma_{A_1} < 10^{-8}$ g/cm^3 · d $0 < \gamma_{A_\beta} < 2 \times 10^{-6}$ g/cm^3 · d. Then, in Fig 5, we plotted the efficacy of treatment after 45 days. Note that the values of $\lambda_{T_1T_r}$ increase along each row, and the values of ζ_{T_β} increase along each column. The ranges of $\lambda_{T_1T_r}$ and ζ_{T_β}, and the ranges of γ_{A_1} and γ_{A_β} include the values that appear in Fig 2.

From Fig 5 we see that (i) for any combination $(\gamma_{A_\beta}, \gamma_{A_1})$, the efficacy increases when $\lambda_{T_1T_r}$ and ζ_{T_β} are decreased. (ii) For large values of $\lambda_{T_1T_r}$ and ζ_{T_β}, tumor progression is likely to occur. (iii) For small values of $\lambda_{T_1T_r}$ and ζ_{T_β}, the efficacy increases as γ_{A_1} and γ_{A_β} are increased. We also see that efficacy always increases if γ_{A_β} is increased. This is not surprising, since if γ_{A_β} is increased, the T_β is decreased and, hence, the killing rate of C by T_8, which is proportional to $1/(1 + \zeta_{T_\beta} T_\beta)$ is increased.

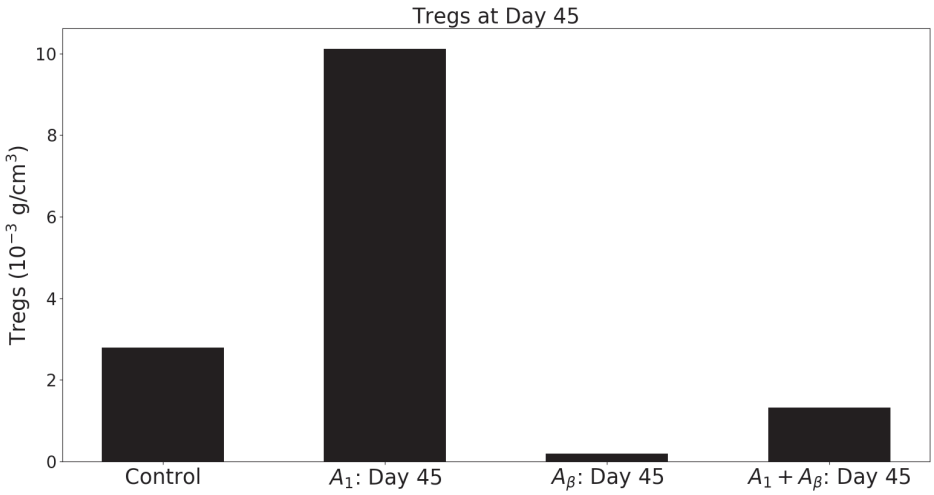

Fig 4. Tregs levels in all treatment combinations with anti-PD-1 and anti-TGF-β. The bar plots represent the density of Tregs in the control, anti-PD-1 only, anti-TGF-β only, and anti-PD-1+anti-TGF-β cases. Tregs increase with anti-PD-1 as single agent, decrease significantly with anti-TGF-β as single agent, and decrease (but remains below the control case) when anti-PD-1 is combined with anti-TGF-β.

https://doi.org/10.1371/journal.pone.0252620.g004

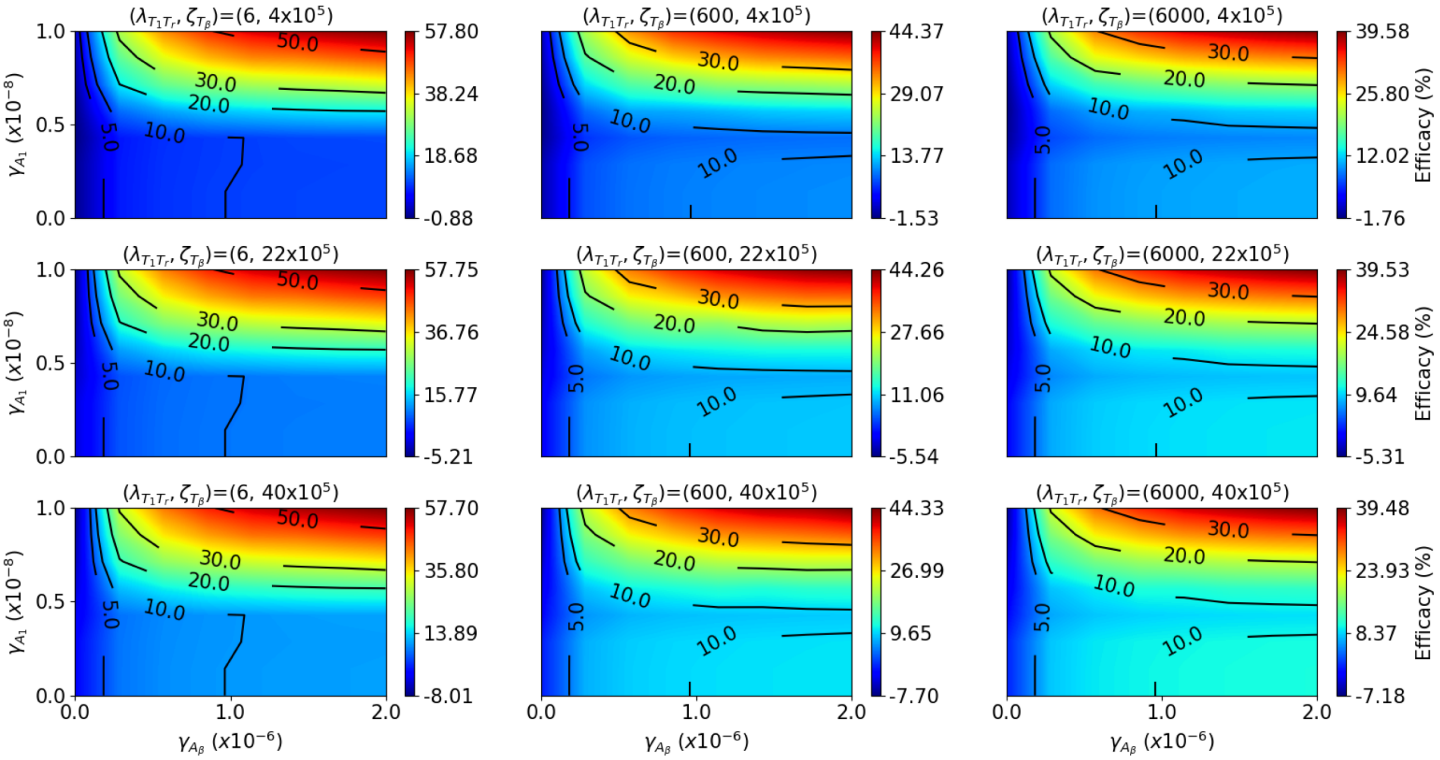

Fig 5. Efficacy map, combination of anti-PD-1 with anti-TGF-β. We vary the cancer-specific parameters $\lambda_{T_1T_r} \in \{6, 6 \times 10^2, 6 \times 10^3\}$d^{-1} and $\zeta_{T_\beta} \in \{4 \times 10^5, 22 \times 10^5, 40 \times 10^5\}$ cm^3/g, and plot efficacy maps for the combination anti-PD-1+anti-TGF-β with doses γ_{A_1} between $0 < \gamma_{A_1} < 10^{-8}$ and γ_{A_β} between $0 < \gamma_\beta < 2\times10^{-6}$ g/cm^3·d, respectively. The color columns indicate the relative difference of the tumor at day 45. Negative values represent anti-PD-1 and anti-TGF-β dose ranges of tumor hyperprogression.

https://doi.org/10.1371/journal.pone.0252620.g005

On the other hand, as seen in the last two columns of Fig 5, for fixed large γ_{A_β}, there is an interval $(\gamma^-_{A_1}, \gamma^+_{A_1})$ such that the efficacy is decreasing as γ_{A_1} increases in this interval. To explain this situation we note that if γ_{A_1} is increased then T_1 and T_8 are increased, but also T_r is increased, at rate $\lambda_{T_1T_r}T_1$, and hence T_β is also increased (by Eq (7)). It follows that the killing rate of C, which is proportional to $T_8/(1+\zeta_{T_\beta}T_\beta)$, may either increase or decrease. Fig 5 shows that, as γ_{A_1} increases, this factor decreases as long as γ_{A_1} remains in an intermediate interval $(\gamma^-_{A_1}, \gamma^+_{A_1})$, and is increased elsewhere.

4 Conclusion

Therapeutic antibodies that block PD-1/PD-L1 induce robust and durable response in some cancer patients, negative response in some patients [12, 14], and no response at all in others [18, 50]. Since substantial proportion of patients have little or no benefits, while treatment with these drugs are costly and might have associated toxicity [51], biomarkers which are likely to predict response rate to PD-1/PD-L1 blockade are highly desirable [51, 52]. You et al. [53] summarizes (in Table 1) clinical outcome of predictive biomarkers for PD-1/PD-L1 blockade, while asserting the need for reliable biomarkers to ensure rational use of this checkpoint blockade. In the present paper we identified two cancer-specific parameters, $\lambda_{T_1T_r}$ and ζ_{T_β}, and used them in a mathematical model to predict the response rate to treatment with anti-PD-1 as single agent and in combination with anti-TGF-β.

Our simulations, in Figs 2 and 4, show agreement with the experimental results (in mice) reported in [15, 22, 23]. We also show, in Fig 3, that under treatment with anti-PD-1 alone, as the parameters $\lambda_{T_1T_r}$ and ζ_{T_β} increase the progression of cancer increases, while treatment does not result in progression of cancer if either $\lambda_{T_1T_r}$ or ζ_{T_β} is small.

The parameters $\lambda_{T_1T_r}$ and ζ_{T_β} can be viewed as biomarkers, predicting the following:

(i) for any combination $(\gamma_{A_\beta}, \gamma_{A_1})$, the efficacy increases when $\lambda_{T_1T_r}$ and ζ_{T_β} are decreased.

(ii) For large values of $\lambda_{T_1T_r}$ and ζ_{T_β}, tumor progression is likely to occur.

(iii) For small values of $\lambda_{T_1T_r}$ and ζ_{T_β}, the efficacy increases as γ_{A_1} and γ_{A_β} are increased.

We also found that while efficacy always inceases when γ_{A_β} is increased, there are regions in the $(\gamma_{A_\beta}, \gamma_{A_1})$-plane such that efficacy is decreased as γ_{A_1} increases: these regions consist of points $\{(\gamma_{A_\beta}, \gamma_{A_1}) : \gamma^-_{A_1} < \gamma_{A_1} < \gamma^+_{A_1}\}$, where $\gamma^-_{A_1}$ and $\gamma^+_{A_1}$ depend on γ_{A_β}.

The mathematical model presented in this paper has several limitations:

1. We assumed that the densities of immature, or naive, immune cells remain constant throughout the progression of the cancer and that dead cells are quickly removed from the tumor.
2. In estimating production parameters we made a steady state assumption in some of the differential equations.
3. Although our mathematical model does not presume any geometric form of the tumor, for simplicity, the simulations have been carried out only in the case of spherical tumor. We note however that spherical cancer models have been used in research as an intermediate between *in vitro* cancer line cultures and *in vivo* cancer [54]. Furthermore, spheroids mirror

the 3D cellular context and therapeutically relevant pathophysiological gradient of *in vivo* tumors [55].

Biomarkers are characteristics of the body and they are critical in order to diagnose a disease and/or to measure the effect of a drug on the patient. In the present paper, based on mice experiments, we developed a mathematical model which demonstrates, depending on two parameters, how primary resistance to anti-PD-1 can be overcome by anti-TGF-beta. These parameters may serve as new cancer biomarkers, but our results will first need to be validated by clinical studies.

Supporting information

S1 File. TGF-β inhibition can overcome cancer primary resistance to PD-1 blockade: A mathematical model. Model equations (Section 1 in S1 File), parameter estimates (Section 2 in S1 File), parameter sensitivity analysis (Section 3 in S1 File), numerical methods used (Section 4 in S1 File) and the parameter values (Tables 1 and 2 in S1 File).
(PDF)

Author Contributions

Conceptualization: Nourridine Siewe, Avner Friedman.

Data curation: Nourridine Siewe, Avner Friedman.

Formal analysis: Nourridine Siewe, Avner Friedman.

Funding acquisition: Nourridine Siewe, Avner Friedman.

Investigation: Nourridine Siewe, Avner Friedman.

Methodology: Nourridine Siewe, Avner Friedman.

Project administration: Nourridine Siewe, Avner Friedman.

Resources: Nourridine Siewe, Avner Friedman.

Software: Nourridine Siewe.

Supervision: Avner Friedman.

Validation: Nourridine Siewe, Avner Friedman.

Visualization: Nourridine Siewe, Avner Friedman.

Writing – original draft: Nourridine Siewe, Avner Friedman.

Writing – review & editing: Nourridine Siewe, Avner Friedman.

References

1. Fares CM, Van Allen EM, Drake CG, Allison JP, Hu-Lieskovan S. Mechanisms of Resistance to Immune Checkpoint Blockade: Why Does Checkpoint Inhibitor Immunotherapy Not Work for All Patients? Am Soc Clin Oncol Educ Book. 2019; 39:147–164. https://doi.org/10.1200/EDBK_240837
2. Ren D, Hua Y, Yu B, Ye X, He Z, Li C, et al. Predictive biomarkers and mechanisms underlying resistance to PD1/PD-L1 blockade cancer immunotherapy. Mol Cancer. 2020; 19(1):19. https://doi.org/10.1186/s12943-020-1144-6 PMID: 32000802
3. Nowicki TS, Hu-Lieskovan S, Ribas A. Mechanisms of Resistance to PD-1 and PD-L1 Blockade. Cancer J. 2018; 24(1):47–53. https://doi.org/10.1097/PPO.0000000000000303
4. Lei Q, Wang D, Sun K, Wang L, Zhang Y. Resistance Mechanisms of Anti-PD1/PDL1 Therapy in Solid Tumors. Front Cell Dev Biol. 2020; 8(672):1–16. https://doi.org/10.3389/fcell.2020.00672

5. Haibe Y, El Husseini Z, El Sayed R, Shamseddine A. Resisting Resistance to Immune Checkpoint Therapy: A Systematic Review. Int J Mol Sci. 2020; 21(17):6176. https://doi.org/10.3390/ijms21176176
6. Togashi Y, Shitara K, Nishikawa H. Regulatory T cells in cancer immunosuppression—implications for anticancer therapy. Nat Rev Clin Oncol. 2019; 16(6):356–371. https://doi.org/10.1038/s41571-019-0175-7
7. Kumagai S, Togashi Y, Kamada T, Sugiyama E, Nishinakamura H, Takeuchi Y, et al. The PD-1 expression balance between effector and regulatory T cells predicts the clinical efficacy of PD-1 blockade therapies. Nat Immunol. 2020; 21(11):1346–1358. https://doi.org/10.1038/s41590-020-0769-3 PMID: 32868929
8. Champiat S, Dercle L, Ammari S, Massard C, Hollebecque A, Postel-Vinay S, et al. Hyperprogressive Disease Is a New Pattern of Progression in Cancer Patients Treated by Anti-PD-1/PD-L1. Clin Cancer Res. 2016; 23(8):1920–1928. https://doi.org/10.1158/1078-0432.CCR-16-1741 PMID: 27827313
9. Champiat S, Ferrara R, Massard C, Besse B, Marabelle A, Soria JC, et al. Hyperprogressive disease: recognizing a novel pattern to improve patient management. Nat Rev Clin Oncol. 2018; 15(12):748–762. https://doi.org/10.1038/s41571-018-0111-2 PMID: 30361681
10. Kato S, Goodman A, Walavalkar V, Barkauskas DA, Sharabi A, Kurzrock R. Hyperprogressors after Immunotherapy: Analysis of Genomic Alterations Associated with Accelerated Growth Rate. Clin Cancer Res. 2017; 23(15):4242–4250. https://doi.org/10.1158/1078-0432.CCR-16-3133
11. Popat V, Gerber DE. Hyperprogressive disease: a distinct effect of immunotherapy? J Thorac Dis. 2019; 11(Suppl 3):S262–S265. https://doi.org/10.21037/jtd.2019.01.97
12. Sabio E, Chan TA. The good, the bad, and the ugly: hyperprogression in cancer patients following immune checkpoint therapy. Genome Med. 2019; 11(1):43. https://doi.org/10.1186/s13073-019-0661-7
13. Denis M, Duruisseaux M, Brevet M, Dumontet C. How Can Immune Checkpoint Inhibitors Cause Hyperprogression in Solid Tumors? Front Immunol. 2020; 11(492):1–8. https://doi.org/10.3389/fimmu.2020.00492
14. Wang X, Wang F, Zhong M, Yarden Y, Fu L. The biomarkers of hyperprogressive disease in PD-1/PD-L1 blockage therapy. Mol Cancer. 2020; 19(81):1–15. https://doi.org/10.1186/s12943-020-01200-x
15. Kamada T, Togashi Y, Tay C, Ha D, Sasaki A, Nakamura Y, et al. PD-1^{+} regulatory T cells amplified by PD-1 blockade promote hyperprogression of cancer. PNAS. 2019; 116(20):9999–10008. https://doi.org/10.1073/pnas.1822001116 PMID: 31028147
16. Bai X, Yi M, Jiao Y, Chu Q, Wu K. Blocking TGF-β Signaling To Enhance The Efficacy Of Immune Checkpoint Inhibitor. Onco Targets Ther. 2019; 12:9527–9538. https://doi.org/10.2147/OTT.S224013
17. Löffek S. Transforming of the Tumor Microenvironment: Implications for TGF- Inhibition in the Context of Immune-Checkpoint Therapy. J Oncol. 2018; 2018(9732939):1–9. https://doi.org/10.1155/2018/9732939
18. Mariathasan S, Turley SJ, Nickles D, Castiglioni A, Yuen K, Wang Y, et al. TGF-β attenuates tumour response to PD-L1 blockade by contributing to exclusion of T cells. nature. 2018; 554(7693):544–548. https://doi.org/10.1038/nature25501 PMID: 29443960
19. Tauriello DVF, Palomo-Ponce S, Stork D, Berenguer-Llergo A, Badia-Ramentol J, Iglesias M, et al. TGFβ drives immune evasion in genetically reconstituted colon cancer metastasis. nature. 2018; 554(7693):538–543. https://doi.org/10.1038/nature25492 PMID: 29443964
20. Ganesh K, Massaguké J. TGFβ Inhibition and Immunotherapy: Checkmate. Immunity. 2018; 48(4):62–628. https://doi.org/10.1016/j.immuni.2018.03.037
21. Sow HS, Ren J, Camps M, Ossendorp F, Ten Dijke PJ. Combined Inhibition of TGF-β Signaling and the PD-L1 Immune Checkpoint Is Differentially Effective in Tumor Models. Cells. 2019; 8(4):320. https://doi.org/10.3390/cells8040320
22. de Streel G, Bertrand C, Chalon N, Liénart S, Bricard O, Lecomte S, et al. Selective inhibition of TGF-β1 produced by GARP-expressing Tregs overcomes resistance to PD-1/PD-L1 blockade in cancer. Nature Communications. 2020; 11(4545):1–15. https://doi.org/10.1038/s41467-020-17811-3 PMID: 32917858
23. Martin CJ, Datta A, Littlefield C, Kalra A, Chapron C, Wawersik S, et al. Selective inhibition of TGFβ1 activation overcomes primary resistance to checkpoint blockade therapy by altering tumor immune landscape. Sci Transl Med. 2020; 12(536):8456. https://doi.org/10.1126/scitranslmed.aay8456 PMID: 32213632
24. Thomas DA, Massagué J. TGF-beta directly targets cytotoxic T cell functions during tumor evasion of immune surveillance. Cancer Cell. 2005; 8(5):369–380. https://doi.org/10.1016/j.ccr.2005.10.012
25. Cai J, Wang D, Zhang G, Guo X. The Role Of PD-1/PD-L1 Axis In Treg Development And Function: Implications For Cancer Immunotherapy. Onco Targets Ther. 2019; 12:8437–8445. https://doi.org/10.2147/OTT.S221340

26. Amarnath S, Mangus CW, Wang JC, Wei F, He A, Kapoor V, et al. The PDL1-PD1 axis converts human TH1 cells into regulatory T cells. Sci Transl Med. 2011; 3(111):111–120. https://doi.org/10.1126/scitranslmed.3003130 PMID: 22133721

27. Whiteside TL. The role of regulatory t cells in cancer immunology. Immunotargets Ther. 2015; 4:159–171.

28. Umansky V, Blattner C, Gebhardt C, Utikal J. The Role of Myeloid-Derived Suppressor Cells (MDSC) in Cancer Progression. Vaccines (Basel). 2016; 4(36):1–16.

29. Fang Z, Wen C, Chen X, Yin R, Zhang C, Wang X, et al. Myeloid-derived suppressor cell and macrophage exert distinct angiogenic and immunosuppressive effects in breast cancer. Oncotarget. 2017; 14881(33):54173–54186. https://doi.org/10.18632/oncotarget.17013 PMID: 28903332

30. Yaseen MM, Abuharfeil NM, Darmani H, Daoud A. Mechanisms of immune suppression by myeloid-derived suppressor cells: the role of interleukin-10 as a key immunoregulatory cytokine. Open Biol. 2017; 10(9):200111. https://doi.org/10.1098/rsob.200111

31. Perrot CY, Javelaud D, Mauviel A. Insights into the transforming growth factor-beta signaling pathway in cutaneous melanoma. Ann Dermatol. 2013; 25(2):135–144. https://doi.org/10.5021/ad.2013.25.2.135

32. Condamine T, Gabrilovich DI. Molecular mechanisms regulating myeloid-derived suppressor cell differentiation and function. Trends Immunol. 2011; 32(1):19–25. https://doi.org/10.1016/j.it.2010.10.002

33. Cantelli G, Crosas-Molist E, Georgouli M, Sanz-Moreno V. TGFb-induced transcription in cancer. Semin Cancer Biol. 2016; 42:60–69.

34. Qi L, Yu H, Zhang Y, Zhao D, Lv P, Zhong Y, et al. IL-10 secreted by M2 macrophage promoted tumorigenesis through interaction with JAK2 in glioma. Oncotarget. 2016; 7(44):71673. https://doi.org/10.18632/oncotarget.12317 PMID: 27765933

35. Steen EH, Wang X, Balaji S, Butte MJ, Bollyky PL, Keswani SG. The role of the anti-inflammatory cytokine interleukin-10 in tissue fibrosis. Adv Wound Care (New Rochelle). 2020; 9(4):184–198. https://doi.org/10.1089/wound.2019.1032

36. Liu Z, Kuang W, Zhou Q, Zhang Y. TGF-β1 secreted by M2 phenotype macrophages enhances the stemness and migration of glioma cells via the SMAD2/3 signalling pathway. Int J Mol Med. 2018; 42(6):3395–3403. https://doi.org/10.3892/ijmm.2018.3923

37. Labbe K, Danialou G, Gvozdic D, Demoule A, Divangahi M, Boyd JH, et al. Inhibition of monocyte chemoattractant protein-1 prevents diaphragmatic inflammation and maintains contractile function during endotoxemia. Critica Care. 2010; 14(R187):1–11. https://doi.org/10.1186/cc9295 PMID: 20950459

38. Kawakami Y, Yaguchi T, Sumimoto H, Kudo-Saito C, Iwata-Kajihara T, Nakamura S, et al. Improvement of cancer immunotherapy by combining molecular targeted therapy. Front Oncol. 2013; 3(136):1–7. https://doi.org/10.3389/fonc.2013.00136 PMID: 23755373

39. Jobe NP, Rösel D, Dvorankova B, Kodet O, Lacina L, Mateu R, et al. Simultaneous blocking of IL-6 and IL-8 is sufficient to fully inhibit CAF-induced human melanoma cell invasiveness. Histochem Cell Biol. 2016; 146(2):205–217. https://doi.org/10.1007/s00418-016-1433-8 PMID: 27102177

40. Oelkrug C, Ramage JM. Enhancement of t cell recruitment and infiltration into tumours. Clin Exp Immunol. 2014; 178(1):1–8. https://doi.org/10.1111/cei.12382

41. Ma Y, Shurin GV, Peiyuan Z, Shurin MR. Dendritic cells in the cancer microenvironment. J Cancer. 2013; 4(1):36–44. https://doi.org/10.7150/jca.5046

42. Choudhry H, Helmi N, Abdulaal WH, Zeyadi M, Zamzami MA, Wu W, et al. Prospects of IL-2 in Cancer Immunotherapy. BioMed Res. 2018; 2018(9056173). https://doi.org/10.1155/2018/9056173 PMID: 29854806

43. Vacaflores A, Freedman SN, Chapman NM, Houtman JCD. Pretreatment of activated human CD8 T cells with IL-12 leads to enhanced TCR-induced signaling and cytokine production. Mol Immunol. 2017; 81:1–15. https://doi.org/10.1016/j.molimm.2016.11.008

44. Obeid E, Nanda R, Fu YX, Olopade OI. The role of tumor-associated macrophages in breast cancer progression (review). Int J Oncol. 2013; 43(1):5–12. https://doi.org/10.3892/ijo.2013.1938

45. Chanmee T, Ontong P, Konno K, Itano N. Tumor-associated macrophages as major players in the tumor microenvironment. Cancers. 2014; 6(3):1670–1790. https://doi.org/10.3390/cancers6031670

46. Chen D, Roda JM, Marsh CB, Eubank TD, Friedman A. Hypoxia inducible factors-mediated inhibition of cancer by gm-csf: a mathematical model. Bull Math Biol. 2012; 74(11):2752–2777.

47. Eubank TD, Roberts RD, Khan M, Curry JM, Nuovo GJ, Kuppusamy P, et al. Granulocyte macrophage colony-stimulating factor inhibits breast cancer growth and metastasis by invoking an anti-angiogenic program in tumor-educated macrophages. Cancer Res. 2009; 69(5):2133–2140. https://doi.org/10.1158/0008-5472.CAN-08-1405 PMID: 19223554

48. Dahmani A, Delisle JB. TGF-β in T Cell Biology: Implications for Cancer Immunotherapy. Cancers (Basel). 2014; 10(194):1–21. https://doi.org/10.3390/cancers10060194

49. Janco JMT, Lamichhane P, Karyampudi L, Knutson KL. Tumor-infiltrating dendritic cells in cancer pathogenesis. J Immunol. 2015; 194(7):2985–2991. https://doi.org/10.4049/jimmunol.1403134

50. Sun JY, Zhang D, Wu S, Xu M, Zhou X, Lu XJ, et al. Resistance to PD-1/PD-L1 blockade cancer immunotherapy: mechanisms, predictive factors, and future perspectives. Biomarker Research. 2020; 8 (35):1–10. https://doi.org/10.1186/s40364-020-00212-5 PMID: 32864132

51. Yi M, Jiao D, Xu H, Liu Q, Zhao W, Han X, et al. Biomarkers for predicting efficacy of PD-1/PD-L1 inhibitors. Mol Cancer. 2018; 17(1):129. https://doi.org/10.1186/s12943-018-0864-3 PMID: 30139382

52. Cottrell TR, Taube JM. PD-L1 and Emerging Biomarkers in Immune Checkpoint Blockade Therapy. Cancer J. 2018; 24(1):41–46. https://doi.org/10.1097/PPO.0000000000000301

53. You W, Shang B, Sun J, Liu X, Su L, Jiang S. Mechanistic insight of predictive biomarkers for antitumor PD-1/PD-L1 blockade: A paradigm shift towards immunome evaluation (Review). Oncol Rep. 2020; 42(2):424–437. https://doi.org/10.3892/or.2020.7643

54. Weiswald B, Bellet D, Dangles-Marie V. Spherical cancer models in tumor biology. Neoplasia. 2015; 17(1):1–15. https://doi.org/10.1016/j.neo.2014.12.004

55. Hirschhaeuser F, Menne H, Dittfeld C, West J, Mueller-Klieser W, Kunz-Schughart LA. Multicellular tumor spheroids: an underestimated tool is catching up again. J Biotechnol. 2010; 148(1):3–15. https://doi.org/10.1016/j.jbiotec.2010.01.012